

Supporting Information

For

Entrapment of metastable nanocrystals by polyoxometalates

*Mark Baranov^{ab}, Yan Duan^a, Nitai Leffler^{ab}, Shani Avineri^{ab}, Vladimir Ezersky^b and Ira A. Weinstock^{*ab}*

^a Department of Chemistry, Ben-Gurion University of the Negev, Beer Sheva, 84105, Israel.

^b Ilse Katz Institute for Nanoscale Science & Technology, Ben-Gurion University of the Negev, Beer Sheva, 84105, Israel.

* E-mail: iraw@bgu.ac.il

S1.1 Experimental Section

All the reagents were of analytical grade and purchased from Alfa Aesar, Sigma Aldrich or Merck and were used without further purification. Type I micropure standard water (18.2 Ω ·cm) was used throughout. Reaction vessels were washed using Milli-Q water and oven-dried prior to use.

For POM synthesis: sodium tungstate dihydrate ($\text{Na}_2\text{WO}_3 \cdot 2\text{H}_2\text{O}$, Sigma Aldrich, ACS reagent, $\geq 99\%$ purity), disodium hydrogen phosphate dihydrate ($\text{Na}_2\text{HPO}_4 \cdot 2\text{H}_2\text{O}$, Merck, analytical grade), sodium bicarbonate (NaHCO_3 , Sigma Aldrich, ACS reagent, $\geq 99.7\%$ purity).

For β -FeOOH precursor synthesis and complex 1 synthesis and purification: iron chloride hexahydrate ($\text{FeCl}_3 \cdot 6\text{H}_2\text{O}$, Alfa-Aesar, ACS reagent, 97.0-102.0% purity), sodium hydroxide (NaOH , Alfa-Aesar, pellets, 98% purity), sodium chloride (NaCl , Sigma Aldrich, AR, $\geq 99.9\%$ purity), Spectrum™ Spectra/Por™ 1 RC Dialysis Membrane Tubing 6000 to 8000 kD MWCO.

For cation exchange and dissolution in organic solvents: n-tetrahexylammonium bromide (THABr, Sigma Aldrich, 99% purity), acetonitrile (MeCN, Sigma Aldrich, HPLC grade, $\geq 99.9\%$ purity), dichloromethane (DCM, Sigma Aldrich, HPLC grade, $\geq 99.8\%$ purity), tetrahydrofuran (THF, Sigma Aldrich, HPLC grade, $\geq 99.9\%$ purity), toluene (Alfa-Aesar, anhydrous, 99.8% purity).

pH Measurements. pH values were measured using a Thermo SCIENTIFIC, ORION STAR A211 pH meter, or a EUTECH INSTRUMENTS, cyberscan pH 11 pH/ mv/ °C Meter. Prior to use, the pH meter was calibrated using standard reference solutions (pH 4.01, 7.00 and 10.01).

Dynamic Light Scattering (DLS). DLS data was collected at 25 °C using a Malvern Zetasizer Nano S90, with size measurement from 0.3nm (diameter) to 5 microns using 90 degree scattering optics. Zetasizer software was used to obtain particle diameter.

Zeta Potential (ZP). Zeta potential measurement was carried out by putting 1.0 mL of solution into measuring cell occupied with two electrodes. Zeta potential data were obtained using a ZEM 3600, Zetasizer, Malvern Instruments Ltd.

Electron Microscopy (TEM, STEM and cryo-TEM). Transmission Electron Microscopy (TEM). Samples for dry TEM and high-resolution TEM and STEM (HRTEM) were prepared by pipetting 5-10 μL of the aqueous sample solution onto Cu grids covered with thin carbon-support films and dried in air. TEM data were obtained using a FEI Tecnai 12 G² electron microscope (120 kV) equipped with a Gatan slow-scan camera. HR-TEM data were obtained using a JEOL JEM-2100F instrument operated at an accelerating voltage of 200 kV.

Cryogenic sample preparation for TEM (cryo-TEM). The cryogenically frozen samples were prepared using a fully automated vitrification device (“Leica”). First, 3 μL of the sample solution were placed by pipette onto a glow discharged 300 Mesh Cu grid covered with a lacey-carbon film, held inside a 100% humidity chamber. The grid was then mechanically “blotted” and immediately plunged into liquid ethane (b.p. 185K) cooled by liquid nitrogen (b.p. 77K). Data were collected on the FEI Tecnai 12 G² instrument (120 kV) and the Gatan slow-scan camera,

using a low-dose regime (to slow down the crystallization of vitrified water and to delay the formation of other artifacts due to beam damage). All images from both dry- and cryo-TEM (including electron diffraction patterns) were analyzed using Digital Micrograph Gatan Inc. software.

Electrospray ionization mass spectra (ESI-MS). Spectra were recorded from an LTQ Orbitrap XL instrument (Thermo Scientific, with an accuracy of 0.1 amu) with a nano spray ion source. TBA⁺ salts of the POM complexes, etched from the surface of the NCs, were dissolved in pure acetonitrile and directly injected for the ESI-MS measurements.

Inductively coupled plasma optical emission spectroscopy (ICP-OES). Elemental analyses were done using an Inductively Coupled Plasma-Optical Emission Spectroscopy ICP-OES (SPECTRO ACROS) analyzer which was calibrated using standard solutions of respective elements.

Raman spectroscopy. Spectra were recorded with a Horiba-Jobin-Yvon Lab Ram HR 800 micro-Raman system, equipped with a Synapse CCD detector using a laser excitation source (532 nm laser) with ND filters. Spectrum of the sample of 6-line ferrihydrite were taken after mild etching of the POM ligands using HCl, the resulting orange precipitate containing the NC cores was used in measurements.

Electron dispersive X-ray spectroscopy (EDS). Analyses were done using a JEOL JEM-2100F TEM operating at 200 kV equipped with a JED-2300T energy dispersive X-ray spectrometer. JEOL Analytical Station software (v. 3.8.0.21) was used for the EDS data analysis.

X-ray photoelectron spectra (XPS). Spectra were obtained using an x-ray photoelectron spectrometer ESCALAB250 ultra high vacuum (10^{-9} bar) apparatus with an Al K α X-ray source and a monochromator with an X-ray beam size of 500 μ m. The survey spectra were recorded with pass energy (PE) of 150 eV and high energy resolution spectra were recorded with PE of 20 eV. All the XPS results were processed using Thermo ScientificTM AVANTAGE software.

Powder X-ray diffraction (PXRD). Patterns were obtained using a Panalytical Empyrean instrument with Cu K α radiation ($\lambda = 1.5418 \text{ \AA}$) operated at 40 kV and 30 mA, and equipped with a position sensitive (PSD) X'Celerator detector.

S1.2 Synthetic methods

Synthesis of Na₇[PW₁₁O₃₉]. Na₇[PW₁₁O₃₉] was prepared according to literary methods¹ and confirmed by IR and NMR spectroscopy.

Synthesis of β -FeOOH nanocrystals. Preparation of the precursor β -FeOOH colloidal solution was based on a previously reported procedure.² Solid FeCl₃·6H₂O (0.542 g, 2.0 mmol) was added under vigorous stirring to a 0.002 M HCl solution (100 mL) at 100 °C. The solution was refluxed while stirring at 100°C for 30 min, followed by cooling to room temperature. The obtained solution is dark red with pH ~1.33.

Synthesis of polyoxometalate complexed ferrihydrite nanocrystals (1). The pH of the as-prepared precursor β -FeOOH solution (7 mL) adjusted to 7.30 by addition of a 0.2 M NaOH solution (2.1 mL) and left to stir. After an hour, 0.75 mL of $\text{Na}_7[\text{PW}_{11}\text{O}_{39}]$ solution (40 mM) was added in a single portion. The pH of the solution decreased to ~ 6.35 after stirring for one hour, after which the pH was fixed to ~ 6.50 using 0.2 M NaOH. The overall volume was fixed to 10 mL and transferred to a Teflon lined stainless-steel reaction vessel and put in an autoclave at 220°C for 24 hours. Upon cooling down to room temperature the contents of the reaction vessel were decanted into a falcon tube, consisting of a precipitate and a light-yellow solution (pH ~ 6.82) that is composed of the desired product, unreacted $[\text{PW}_{11}\text{O}_{39}]^{7-}$ and a by-product and of monosubstituted Fe-POM, $[\text{PFeW}_{11}\text{O}_{39}]^4$. The main product, **1**, was separated from solution by precipitation through the addition of NaCl (final conc. 2M), followed by centrifugation, resulting in a brown pellet. After centrifugation, the supernatant was discarded and the pellet was re-dissolved in pure water. This precipitation and dissolution processes was carried out a total of three times in order to remove any remaining contaminants, and finally dialyzed against water for 24 hours (final pH ~ 5.90). The final product is an optically clear brown solution containing **1**. Yield (~ 25 mL solution): 0.098 g, 40.1% based on Fe content (from ICP-OES).

Cation exchange procedure

The concentration of the POMs in a solution of **1** was determined based on the amounts and ratio of W : Fe obtained from ICP-OES and the size of the nanoparticles obtained from TEM/XRD (see Table S1). Considering an average crystallite size of 4.92 nm from Scherrer analysis (see Fig. S15), the density and molar mass of ferrihydrite (consistent with the unit cell contents of ferrihydrite given by Eggleton³), we have obtained the concentration of POMs in solution as follow:

Given that: $r_{NC} = 2.46$ [nm], density $\rho(FH) = 3.45 \cdot 10^{-21}$ [g nm⁻³], $M.W.(FH) = 148.13$ [g mol⁻¹]

- Volume of a single NC as a sphere, $v_{NC} = 62.3$ [nm³], with the above density and M.W., we obtain:

$$\#Fe \text{ atoms per NC} = \frac{v_{NC} \cdot \rho(FH) \cdot N_A}{M.W.(FH)} = \frac{62.3 \text{ [nm}^3\text{]} \cdot 3.45 \cdot 10^{-21} \left[\frac{\text{g}}{\text{nm}^3} \right] \cdot 6.023 \cdot 10^{23} \left[\frac{\text{Fe atoms}}{\text{mol}} \right]}{148.13 \left[\frac{\text{g}}{\text{mol}} \right]}$$

$$\#Fe \text{ atoms per NC} = 874 \text{ [Fe atoms]}$$

- From the ICP-OES ratio of 74.5 : 25.5 percent Fe : W, one obtains an average of 299 W atoms per NC, consistent with ca. 27 POMs each containing 11 W atoms.
- Additionally, from ICP-OES one obtains the ppm concentration (mg/L) of Fe, which is readily converted to molar concentration. In the solution used for the cation exchange procedure, we have obtained a concentration of [Fe] (as ferrihydrite) of $2.1 \cdot 10^{-3}$ M, and as each NC contains 874 Fe atoms on average, immediately we obtain that the concentration of NCs in solution as $2.4 \cdot 10^{-6}$ M, and as 27 POMs are bound on average to each particle, the concentration of POMs is $6.5 \cdot 10^{-5}$ M.

Next, sub-stoichiometric (relative to the calculated POM concentration, as shown above, and considering a -4 charge per POM) addition of tetrahexylammonium bromide (THABr, 3 mM solution of which 2 mL were added, $n(\text{THABr}) = 1.5 \cdot 10^{-6}$ mol) to a solution containing **1** (25 mL solution of **1**, $n(\text{POM}) = 1.63 \cdot 10^{-6}$ mol) results in the formation of an oily orange precipitate (see Figure S9). The use of sub-stoichiometric amount of THABr was done in order to prevent excess of counter-cations upon dissolution in MeCN. Centrifugation of the cloudy solution allows separation of an orange pellet from the solution, with the supernatant containing some leftover **1** that did not undergo cation exchange. Next, the supernatant is separated from the pellet, which is subsequently redissolved in analytical grade (99%+) MeCN. A concentration of $0.047 \text{ g} \cdot \text{mL}^{-1}$ can be readily achieved and used as a stock solution for transfer into other organic solvents. Dynamic light scattering of the solution shows a number weighted diameter of ca. 13 nm, with a small population at ca. 38 nm. Phase stability of **1** in MeCN was investigated using PXRD, cryo-TEM and SAED (see Figures S10-S12), showing no change of the 6-line ferrihydrite phase upon transfer to MeCN. The solution is stable for months at room temp. and can be stored in a refrigerator ($4 \text{ }^\circ\text{C}$).

Dissolution of 1 in THF, DCM and toluene

The solution of **1** in MeCN can be used as a stock solution for insertion of **1** into other organic solvents. Specifically, 0.187 g of the THA form of **1** was dissolved in 4 mL MeCN, resulting in a clear, deep, brown colored solution. A 50 μL aliquot of the stock solution was added to: a) 950 μL of tetrahydrofuran (THF), b) mixture of 150 μL MeCN and 800 μL dichloromethane (DCM), c) mixture of 200 μL MeCN and 750 μL toluene. The solution of **1** in 95% v/v THF and 80% v/v DCM are stable for months, while the solution in 75% v/v toluene is stable for several weeks. Dynamic light scattering of the solution shows a trend consistent with the polarity of the solvents, showing number weighted radius averages of ca 4.8, 16.6 and 41.1 nm for THF, DCM and toluene, respectively (see Figure S13).

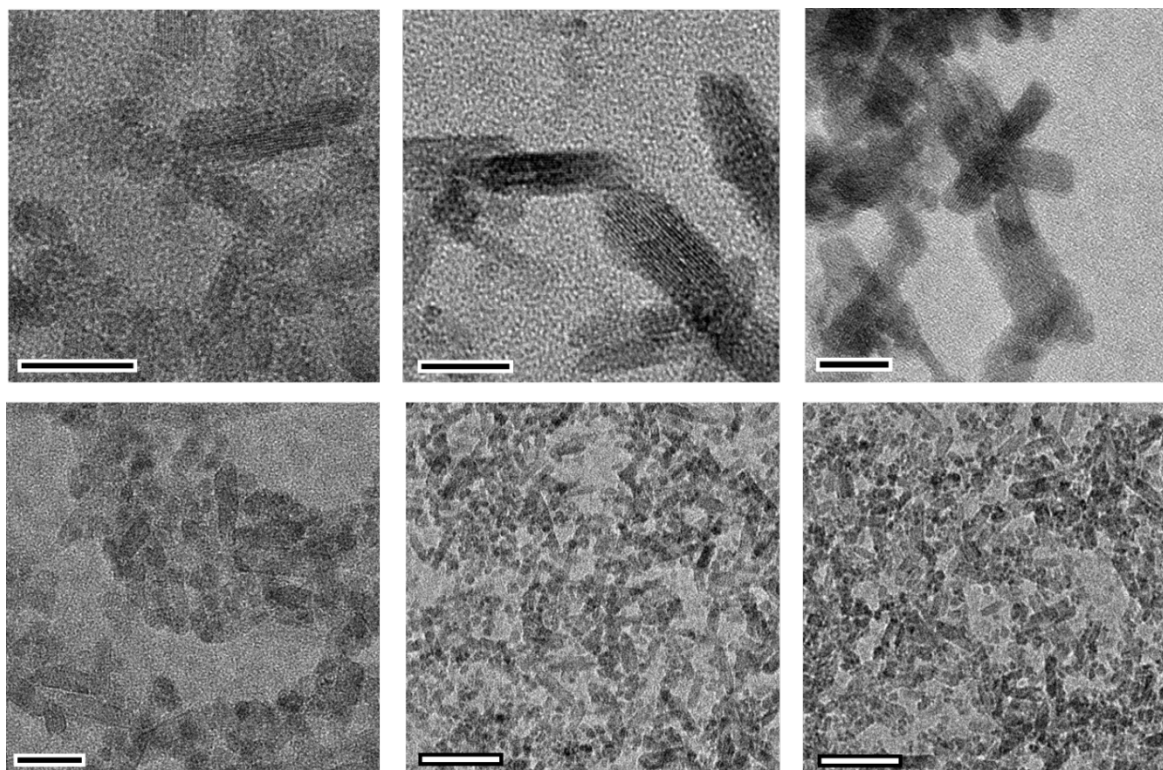


Figure S1. TEM images of precursor β -FeOOH nanorods. Scale bars; black w/ white border – 20 nm, white w/ black border – 50 nm

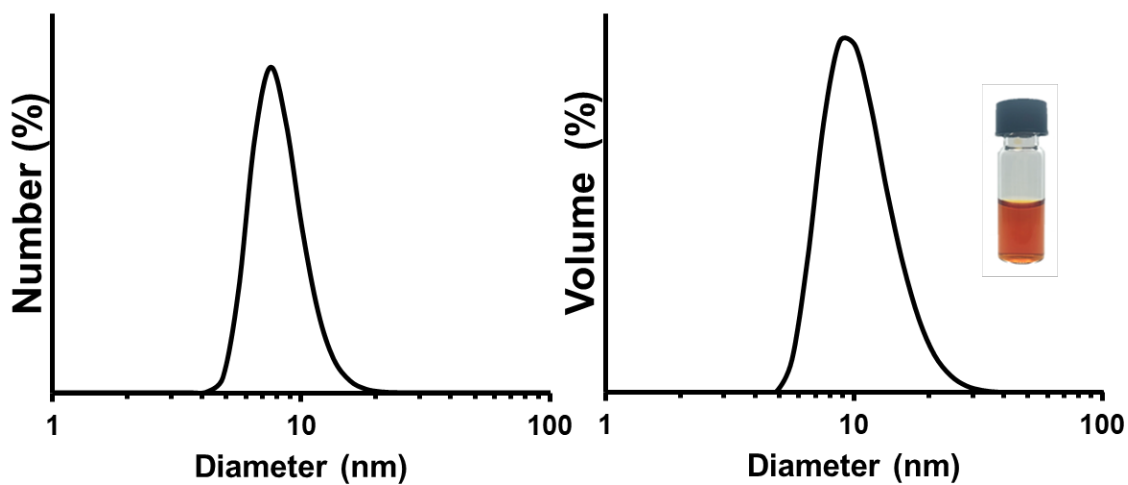


Figure S2. Dynamic light scattering data of **1**. Number weighted (left) and volume weighted (right) of an optically clear solution of **1** (inset) corresponding to average hydrodynamic diameters of ca. 8.1 and 10.2, respectively.

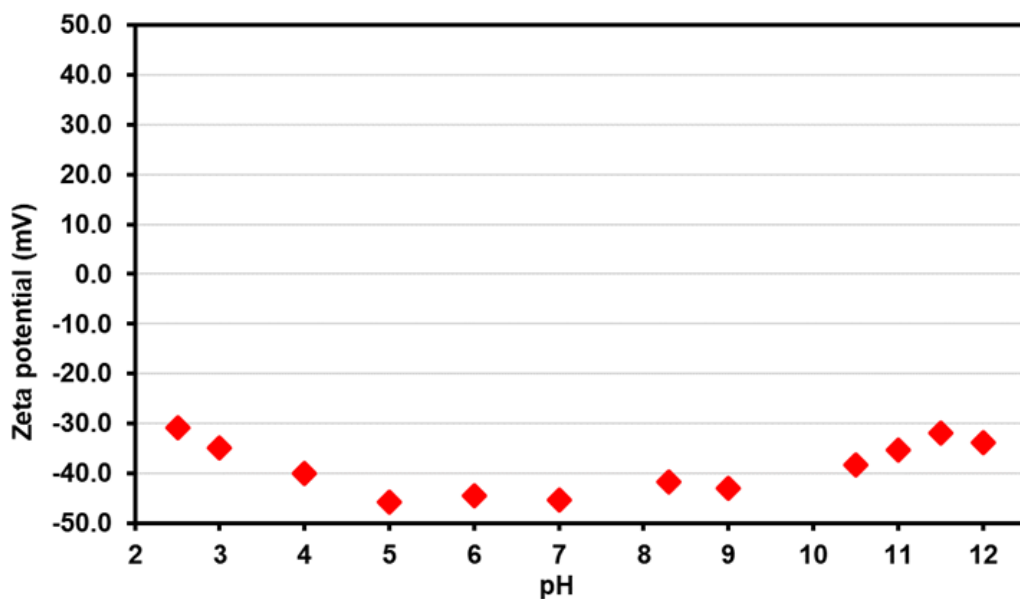


Figure S3. Zeta potential measurements of **1** across a wide pH range, showing a consistent negative potential ranging between -31 to -45 mV throughout. The negative potential is consistent with the presence of POMs on the surface of the ferrihydrite NCs, imparting stability to aggregation and precipitation. For comparison, the isoelectric point of ferrihydrite is located at pH 8.4-8.5.

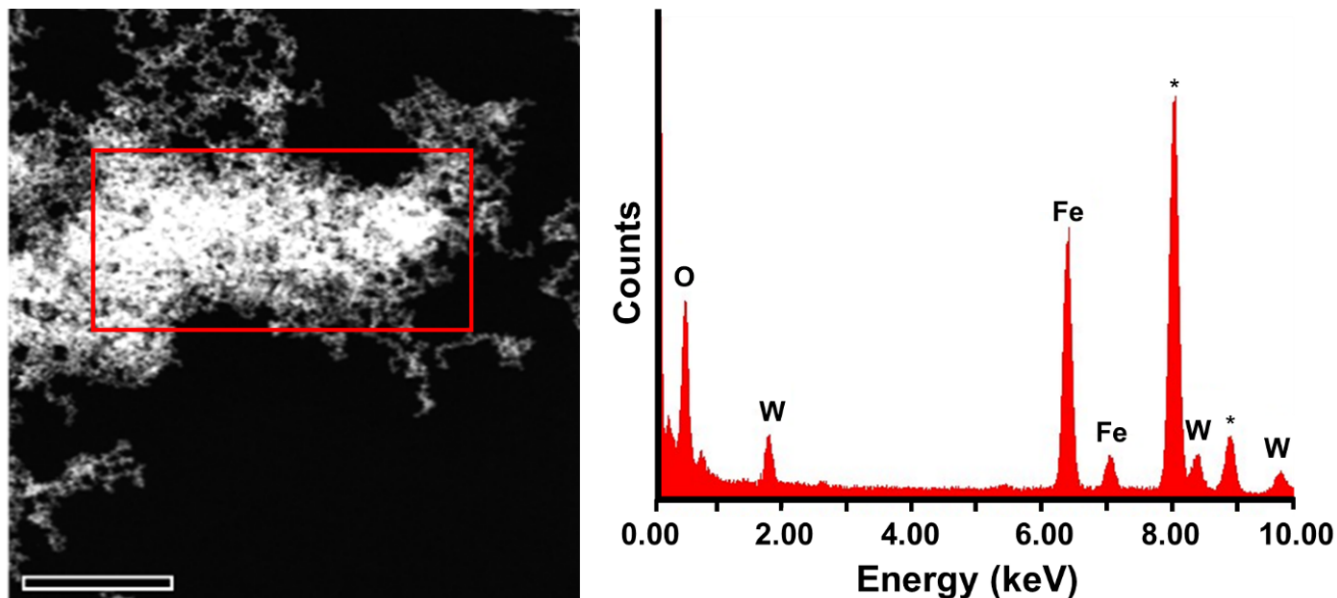


Figure S4. EDS spectrum of a selected area containing **1** (red square), showing the presence of oxygen, tungsten and iron (with a Cu signal from the TEM grid, marked in asterisk). Scale bar – 200 nm.

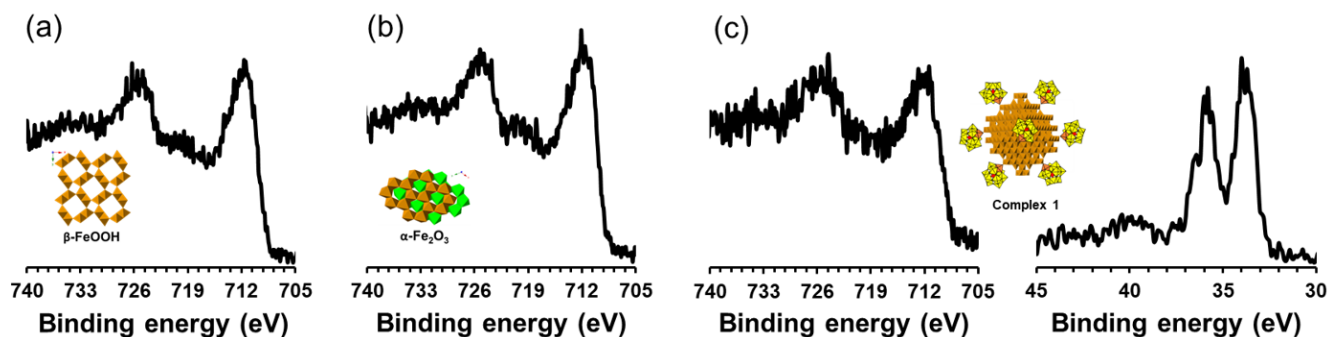


Figure S5. High resolution XPS spectra of: (a) Fe2p region of the β -FeOOH precursor. (b) Fe2p region of the hydrothermal product obtained without POMs, α -Fe₂O₃. (c) Left – Fe2p region of **1**, right – W4f region of **1**. The Fe2p region of (a-c) are consistent with Fe(III) in the samples, while the W4f region of (c) is consistent with W(VI) in the sample.

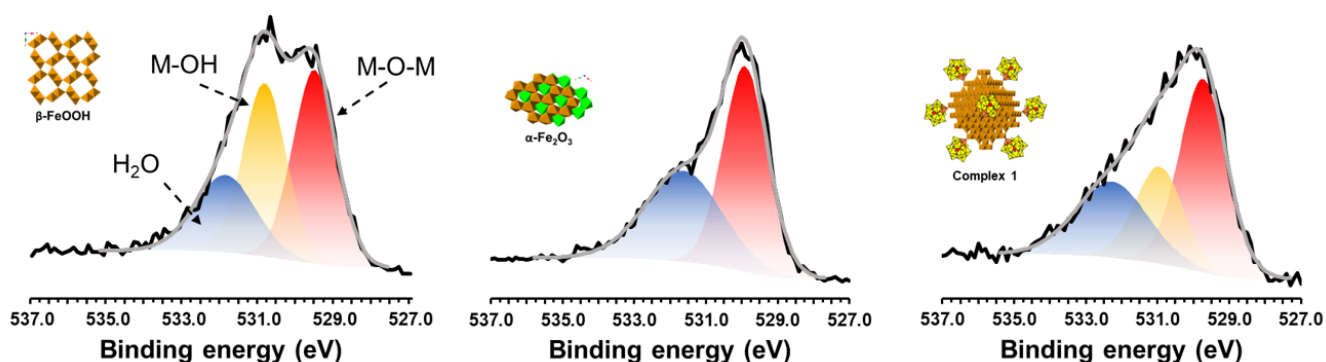


Figure S6. High resolution XPS spectra of the O1s region of: left – β -FeOOH, center – α -Fe₂O₃, right – **1**. Deconvolution of the spectra shows that in the precursor (β -FeOOH) there is an equimolar distribution of hydroxide (yellow traces - M-OH; 530.85-530.94 eV) and oxide (red traces - M-O-M; 529.54-529.92 eV) with some adsorbed water (blue traces – H₂O; 531.62-532.26 eV), while in complex **1** there is a noticeable increase in the oxide content due to the POM ligands, each for a total of 39 terminal and bridging oxo groups. On the other hand, the hydrothermal product obtained without POMs, α -Fe₂O₃, completely lacks a hydroxide signal.

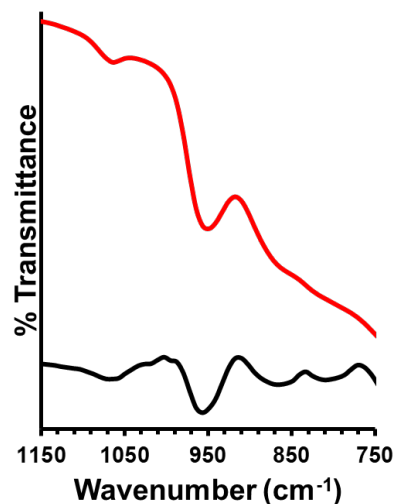


Figure S7. Baseline correction of the FTIR spectrum of **1**. The unprocessed (i.e., non baseline corrected) FTIR spectrum of **1** (red curve), a pronounced absorbance from the small NC cores is starting from approx. 910 cm^{-1} and increases to a maximum absorbance (smaller %-transmittance) at 750 cm^{-1} . This effect has been observed in previous cases when POMs were bound to metal oxide, oxyhydroxide and hydroxide nanocrystals ⁴⁻⁷. Baseline correction was used to obtain the black curve, allowing the relatively weaker intensity bands stemming from the POM ligands around $910\text{-}750\text{ cm}^{-1}$ to be more clearly resolved. The black curve is included in Fig. 3 in the main text.

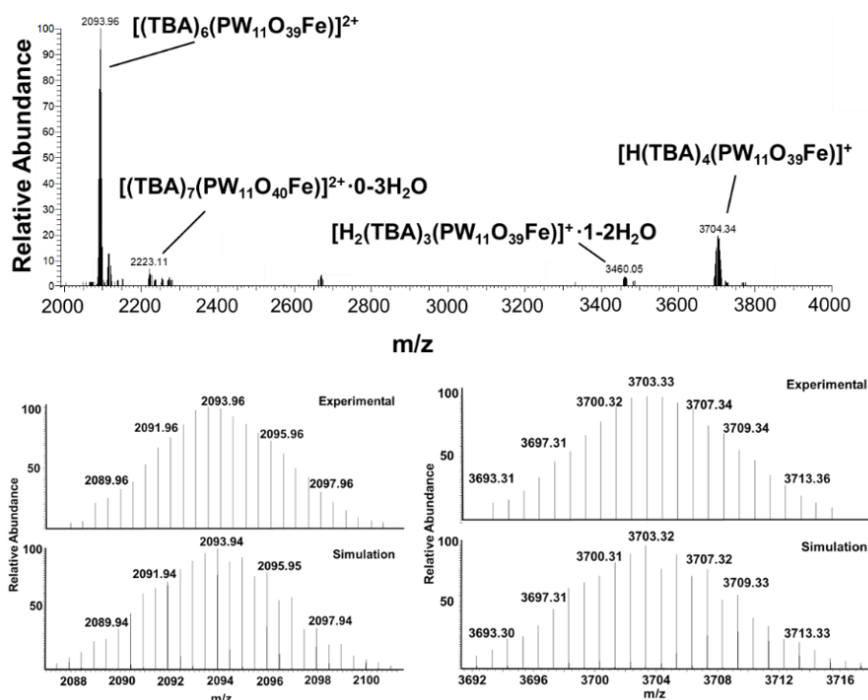


Figure S8. Top shows the ESI-MS spectrum of the supernatant remaining after cleaving the POM ligands off the ferrihydrite surface through hydrolysis with acid. Two dominant peak envelopes (experimental and simulated spectra at bottom) are observed at $m/z = 3704.34$ and 2093.96 , corresponding to $[\text{H}(\text{TBA})_4(\text{PW}_{11}\text{O}_{39}\text{Fe})]^+$ and $[(\text{TBA})_6(\text{PW}_{11}\text{O}_{39}\text{Fe})]^{2+}$, respectively. Other minor peaks were assigned to various other chemical species.

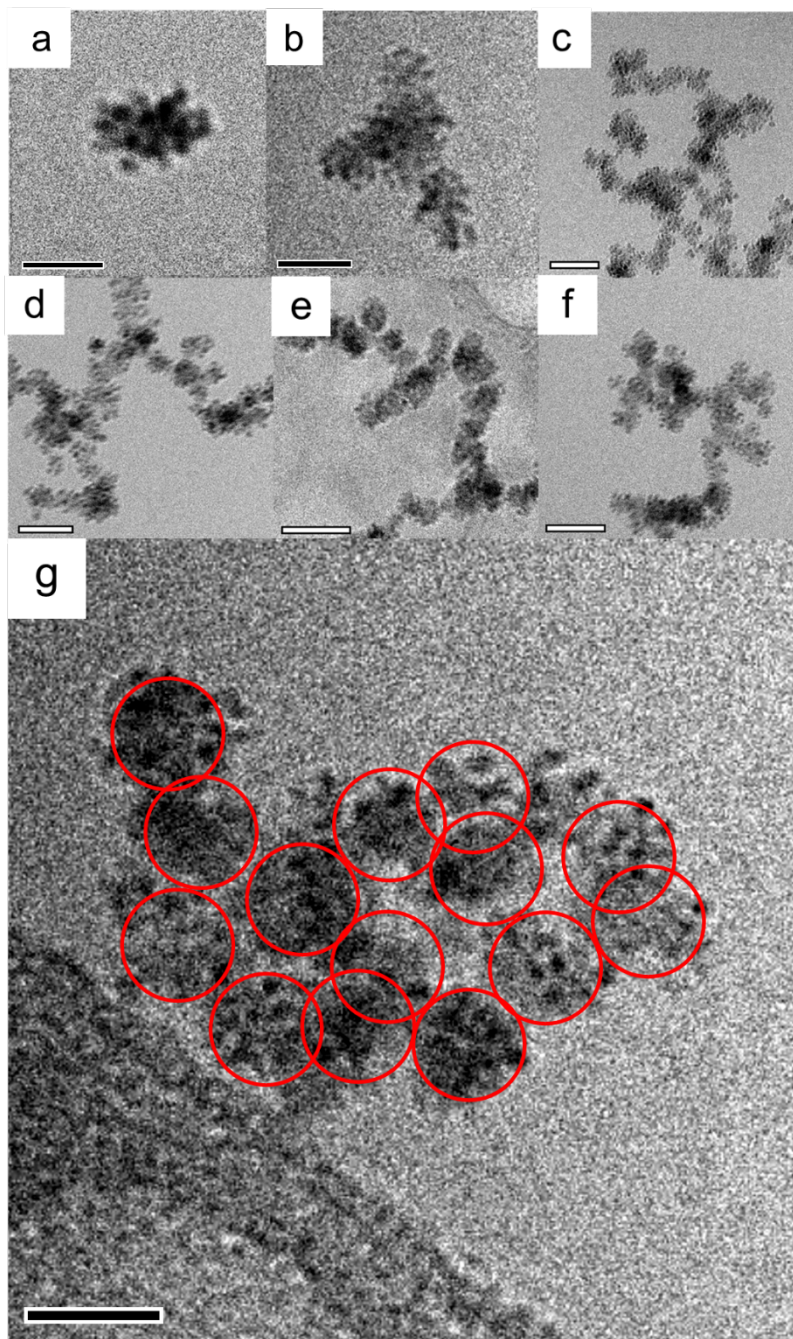


Figure S9. Cryo-TEM images of **1**. (a) Individual particle, with visible POM ligands on the surface of the NC core. (b) Several particles clustered together. Such clustering occurs due to ion-pairing interactions between alkali metals in the solution (part of the charge balance of each NP) and the highly negatively charged POM ligands. (c-g) Clusters of particles, with the particles in image (g) highlighted by red circles. Scale bars; (a-b, g) – 10 nm, (c-f) – 20 nm

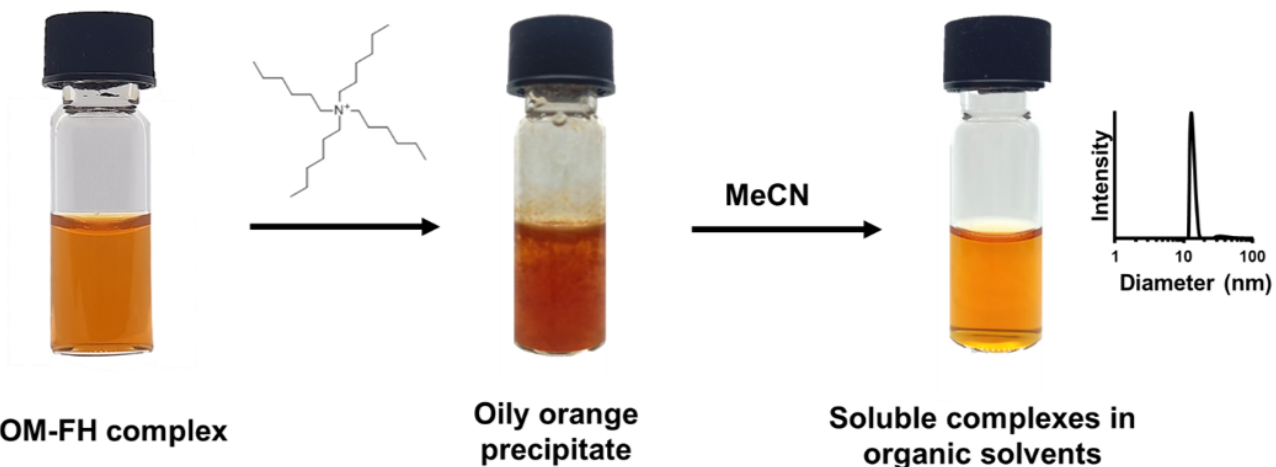


Figure S10. Schematic representation of the cation exchange in **1**. Addition of tetrahexylammonium bromide forms an oily orange precipitate, which, upon isolation, is readily dissolved in acetonitrile. Inset on the right is the number weighted DLS diameter of **1** in MeCN, with the main population at ca. 13 nm, and a small population at ca. 38 nm.

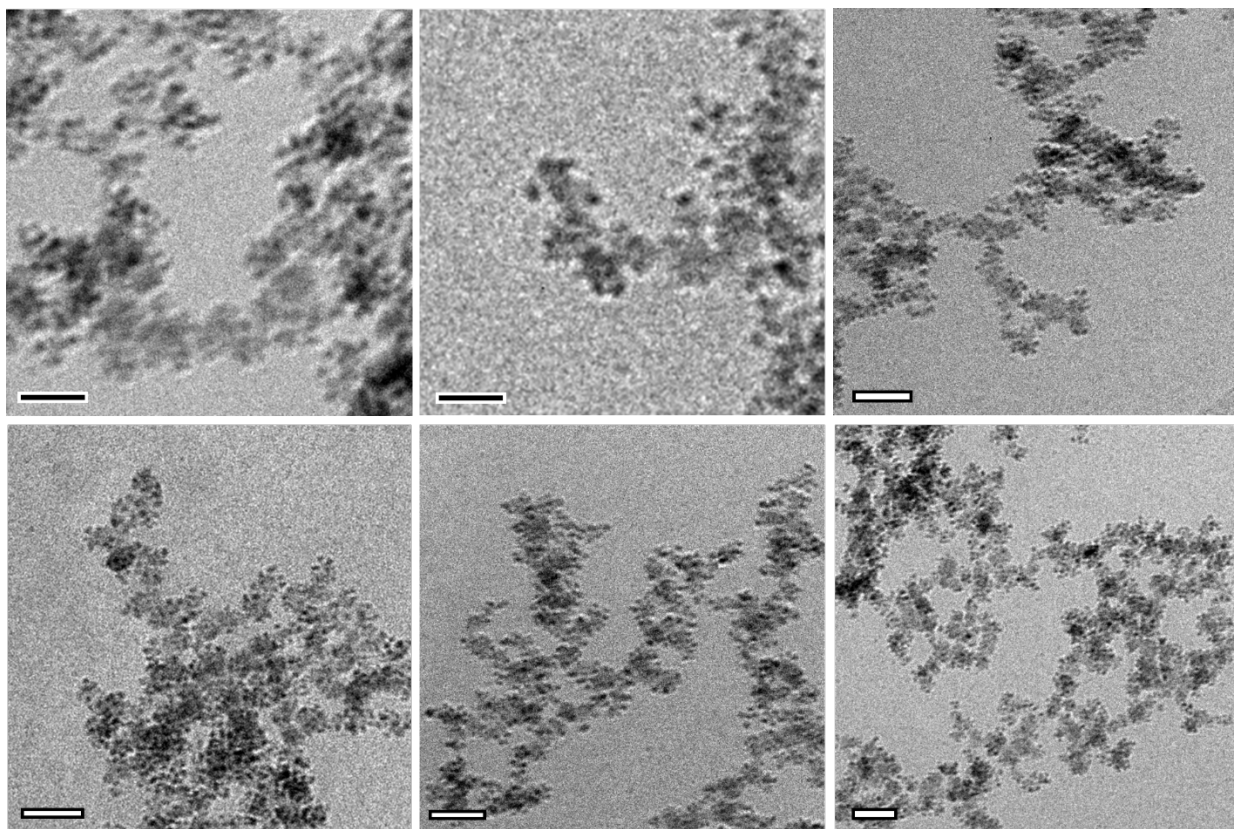


Figure S11. Cryo-TEM images of **1** in acetonitrile. The POM ligands are visible on the surface of the nanocrystalline cores. Particle clustering occurs due to ion-pair interactions with THA^+ resulting from the high negative charge on the particles, ca. -124 per particles based on an average calculated coverage of 27 POMs per core. Scale bars - black w/ white border – 10 nm, white w/ black border – 20 nm

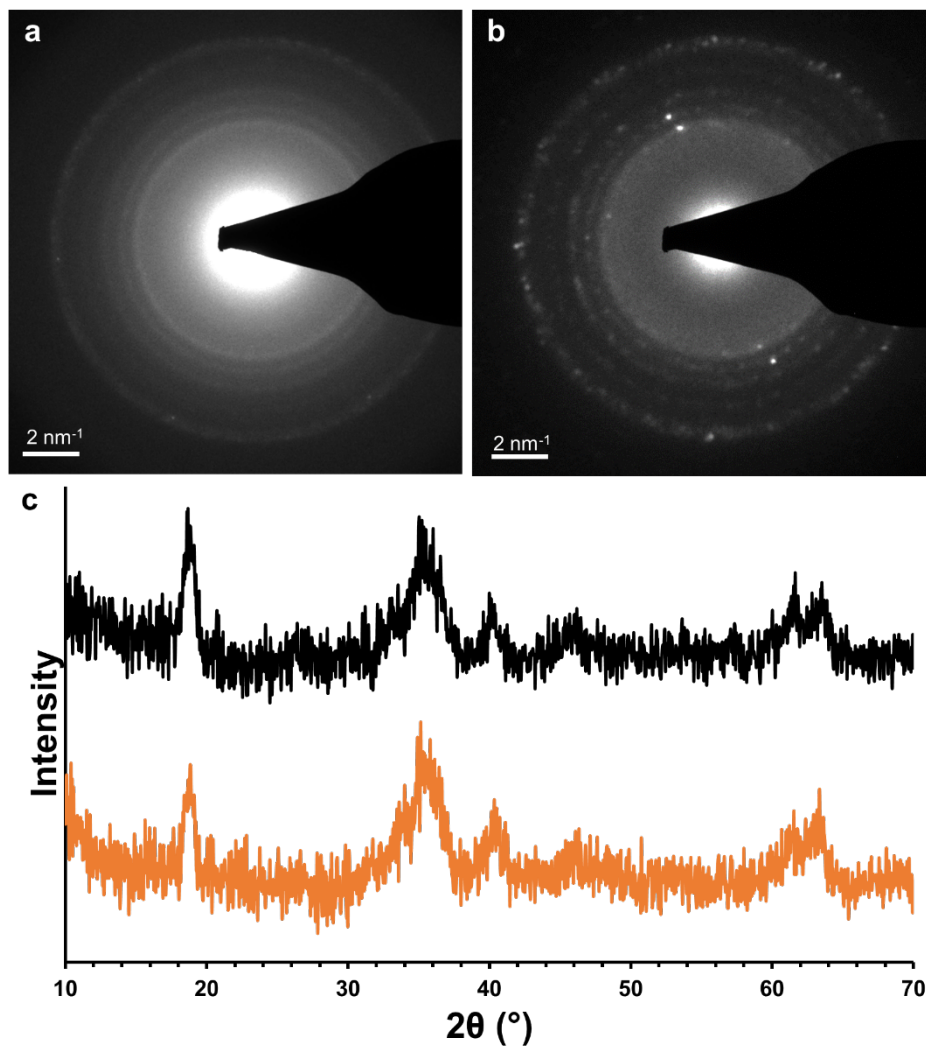


Figure S12. Core characterization post cation exchange. (a-b) Comparison between the selected area diffraction patterns of **1** in (a) water, (b) acetonitrile. (c) PXRD patterns of **1** in aqueous form (top, black trace) and organic form (bottom, orange trace).

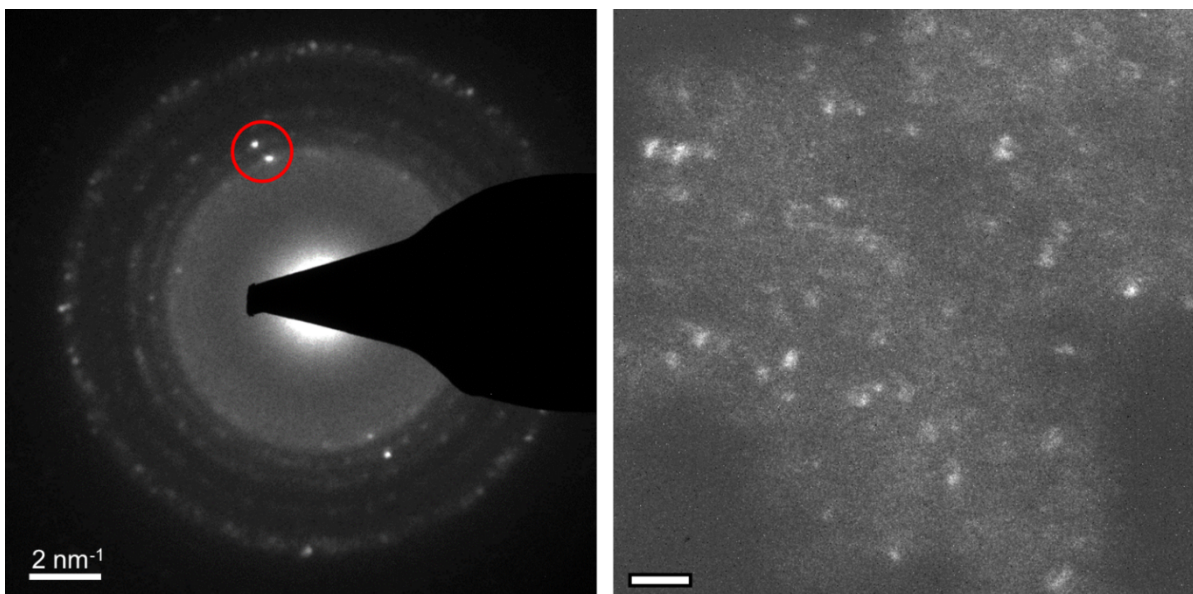


Figure S13. Dark field imaging of the diffraction spots circled in red. The small nanocrystalline cores of **1** are readily observed as the “illuminated” areas. Scale bar – 20 nm.

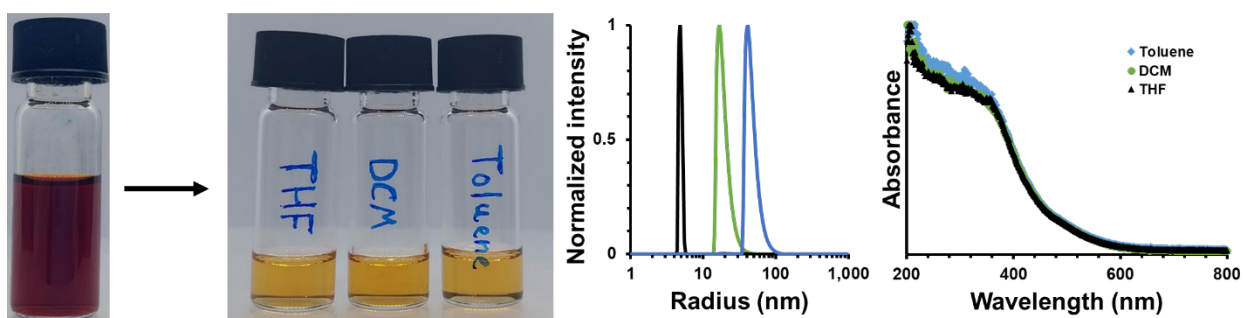


Figure S14. Insertion of **1** into various organic solvents. On the left is a stock solution of **1** in MeCN ($0.047 \text{ g}\cdot\text{mL}^{-1}$ of the THA form of **1**), from which $50 \mu\text{L}$ aliquots were added to THF, DCM and toluene. The DLS data shows that number weighted radii of ca. 4.8, 16.6 and 41.1 nm for THF (black trace), DCM (green trace) and toluene (blue trace), respectively. The UV-vis spectrum of **1** in the aforementioned solutions is shown, practically identical for all three cases.

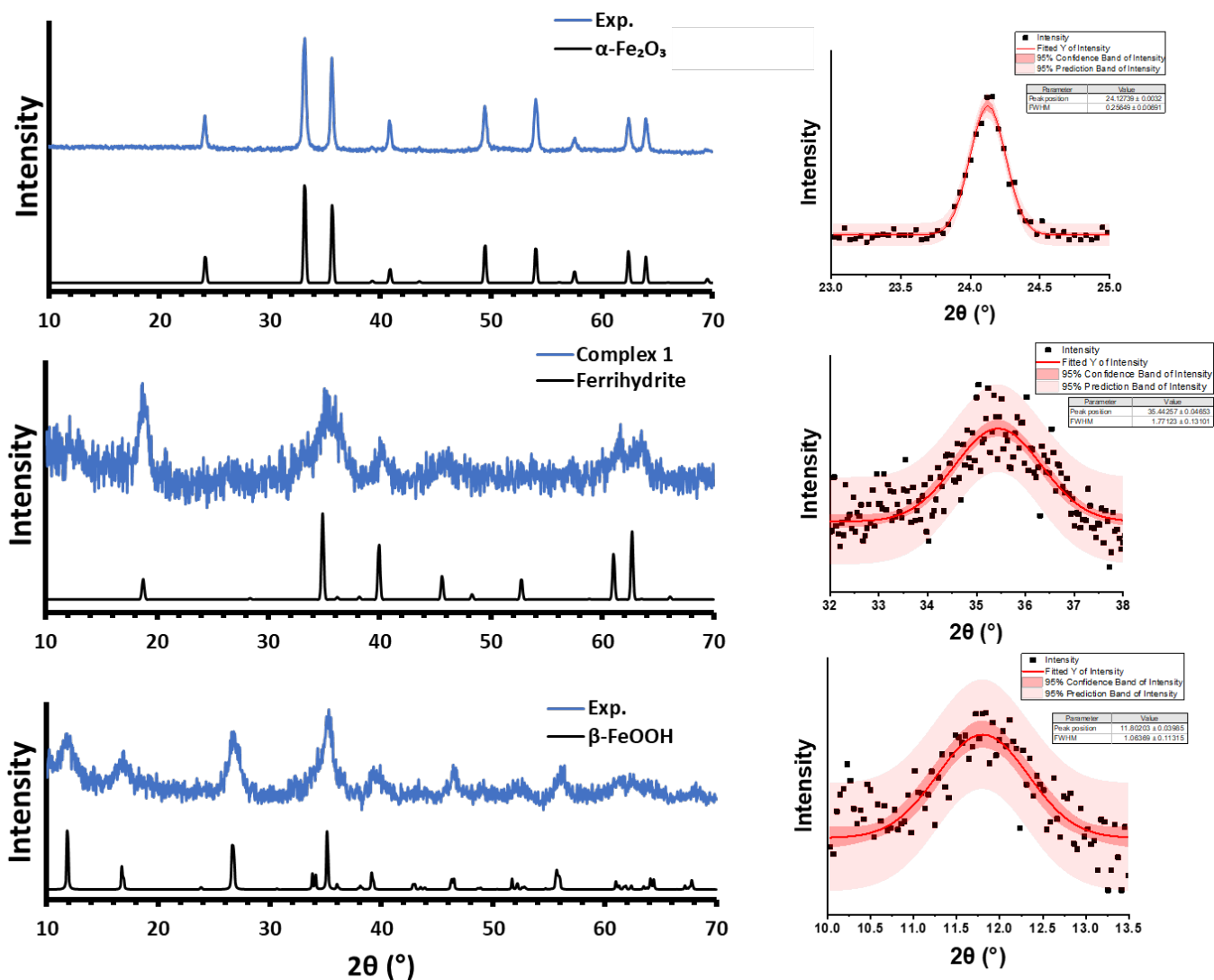


Figure S15. PXRD spectra, both experimental and simulated, and Scherrer analysis (curves on the right). Top – obtained product when β -FeOOH was hydrothermally treated at 220°C for 24 h *without* POM, matching that of α -Fe₂O₃ with an average crystallite size of 66.3 nm. Middle – obtained product from hydrothermal treatment (same conditions as top) *with* POM, complex **1**, with an average crystallite size of 4.92 nm. Bottom – the precursor β -FeOOH used, with an average crystallite size of 7.87 nm.

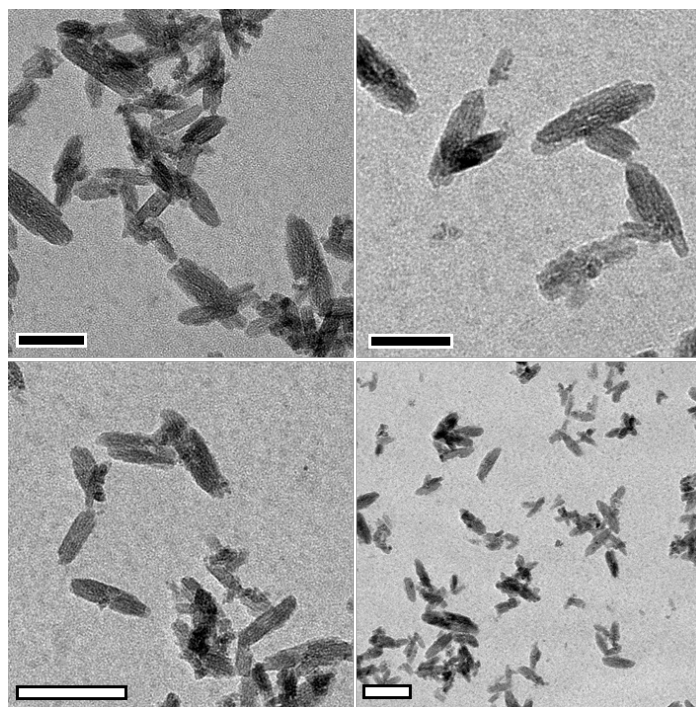


Figure S16. TEM images showing the morphology of the α - Fe_2O_3 nanorods obtained after hydrothermal treatment of β - FeOOH without POM ligands. Scale bars – black w/ white border – 50 nm, white w/ black border – 100 nm.

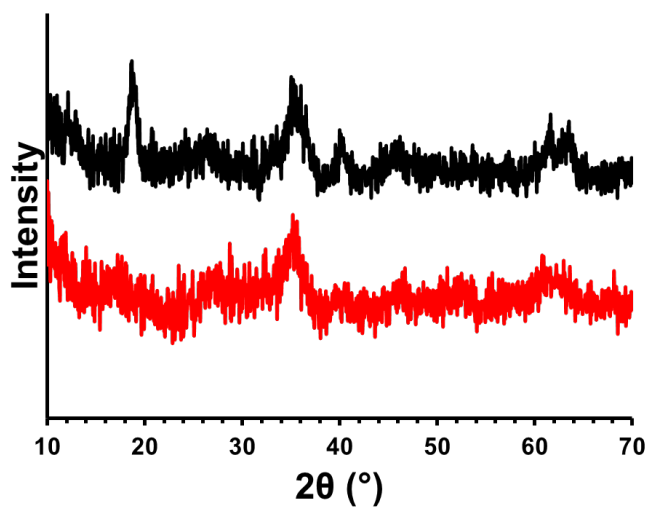


Figure S17. PXR D spectra of the products obtained from hydrothermal treatment of β - FeOOH nanorods. Top: product **1**, obtained at 220°C for 24 h, showing the characteristic peaks of 6-line ferrihydrite. Bottom: product obtained at 80°C for 6 h, showing the characteristic peaks of 2-line ferrihydrite, a poorly ordered 6-line ferrihydrite.

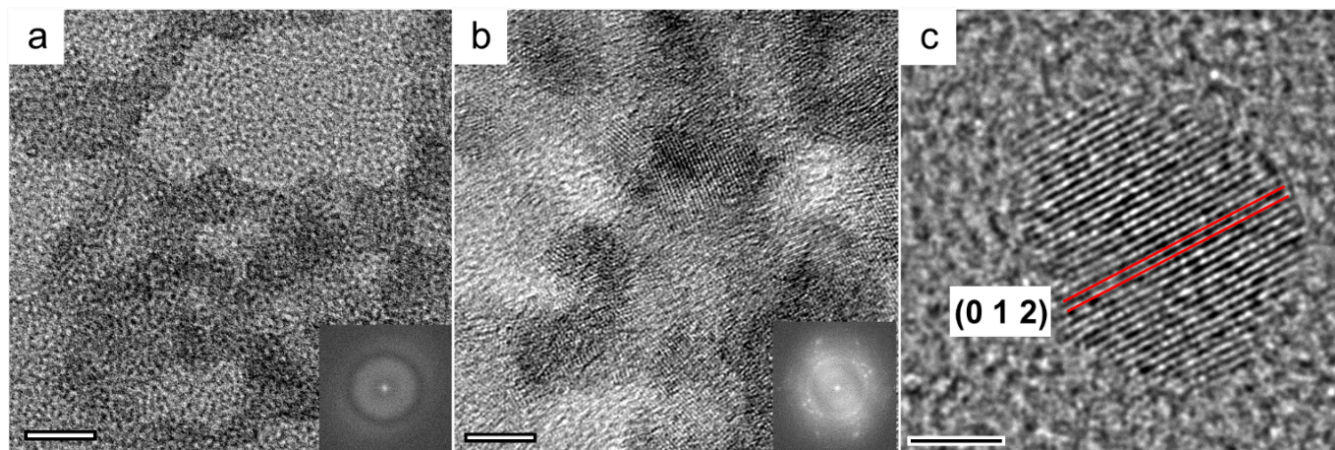


Figure S18. High resolution TEM imaging of **1** under different hydrothermal conditions. (a) Resulting particles under 80°C for 6 h, a poorly crystalline material (identified by PXRD as 2-line ferrihydrite) as shown by FFT (inset). (b) Resulting particles under 220°C for 24 h, clearly showing facets of a highly crystalline material (identified by PXRD as 6-line ferrihydrite), with FFT showing high periodicity (inset). (c) Zoom in on an individual particle of **1**, same synthetic conditions as in (b), showing the facets corresponding to the (0 1 2) Miller index of 6-line ferrihydrite. Scale bars – (a-b) 5 nm; (c) 2 nm.

Table S1. Calculation of atomic-fractions of Fe and W of **1**, considering a 4.92 nm (Diameter) ideal spherical ferrihydrite NC core and 2.8 nm² POM footprint on its surface.

[Fe] (as ferrihydrite)	0.0021 M
Density of ferrihydrite	$3.45 \cdot 10^{-21}$ g nm ⁻³
Mol. Wt. of ferrihydrite (as Fe ₅ O ₃ (OH) ₉)	148.13 g mol ⁻¹
Volume of ferrihydrite sol.	0.027 L
Moles of Fe	$5.67 \cdot 10^{-5}$ mol
Volume of one particle	62.3 nm ³
No. of Fe atoms per particle	874
Surface area of one particle	76 nm ²
POM footprint	2.8 nm ²
No. of POMs per particle	27
Sum of W + Fe atoms / particle	1173
Atom/atom fraction of Fe	0.74
Atom/atom fraction of W	0.26
[Ferrihydrite] particles	$2.4 \cdot 10^{-6}$ M
[POM] bound to NCs	$6.5 \cdot 10^{-5}$ M

References

1. M. Baranov, T. Tubul, Y. Azulai and I. A. Weinstock, *Inorg. Chem.*, 2019, **58**, 8877-8883.
2. L. S. Timothy, L. B. Bronwyn, K. B. Nicholas, W. Christopher, Y. Max and E. O. Frank, *J. Photonics Energy*, 2016, **7**, 1-12.
3. R. A. Eggleton and R. W. Fitzpatrick, *Clays Clay Miner.*, 1988, **36**, 111-124.
4. B. Chakraborty, G. Gan-Or, M. Raula, E. Gadot and I. A. Weinstock, *Nat. Comm.*, 2018, **9**, 4896.
5. Y. Duan, B. Chakraborty, C. K. Tiwari, M. Baranov, T. Tubul, N. Leffler, A. Neyman and I. A. Weinstock, *ACS Catal.*, 2021, **11**, 11385-11395.
6. T. Tubul-Sterin, M. Baranov, G. Gan-Or, N. Leffler, A. Neyman and I. A. Weinstock, *Inorg. Chem.*, 2022, **62**, 1804-1812.
7. M. Raula, G. Gan Or, M. Saganovich, O. Zeiri, Y. Wang, M. R. Chierotti, R. Gobetto and I. A. Weinstock, *Angew. Chem., Int. Ed.*, 2015, **54**, 12416-12421.